PCCP

PAPER

View Article Online
View Journal | View Issue

Cite this: *Phys. Chem. Chem. Phys.*, 2018, **20**, 22719

Boron-based binary $Be_6B_{10}^{2-}$ cluster: three-layered aromatic sandwich, electronic transmutation, and dynamic structural fluxionality†

Lin-Yan Feng,[a] Jin-Chang Guo,[ab] Peng-Fei Li[a] and Hua-Jin Zhai *[a]

Boron-based nanoclusters have unique structures, bonding, and dynamic properties, which originate from boron's electron-deficiency. We demonstrate here that pouring in extra electrons can alter such systems fundamentally. A coaxial triple-layered $Be_6B_{10}^{2-}$ sandwich cluster is designed *via* global structural searches and quantum chemical calculations. It is well defined as the global minimum, which consists of a slightly elongated B_{10} monocyclic ring and two Be_3 rings, the latter forming a Be_6 trigonal-prism albeit without interlayer Be–Be bonding. The B_{10} ring shows structural and chemical integrity with respect to the Be_3 rings, and yet it differs markedly from the free B_{10} cluster and closely resembles the C_{10} cluster. The present data testify to the idea of electronic transmutation, in which a B^- is equivalent to C and a B_{10} cluster, upon charge-transfer, is converted to and stabilized as a monocyclic ring analogous to C_{10}. Chemical bonding analyses reveal that the B_{10} ring in the $Be_6B_{10}^{2-}$ cluster has 10π and 10σ delocalization and each Be_3 ring is held together by 2σ electrons, collectively rendering four-fold π/σ aromaticity. The bonding pattern is in line with the formula of $[Be_3]^{4+}[B_{10}]^{10-}[Be_3]^{4+}$, suggesting a highly charged electron-transfer complex. Furthermore, the $Be_6B_{10}^{2-}$ cluster is dynamically fluxional with dual modes of revolution (orbiting) and rotation (twisting), being structurally robust at least up to a temperature of 1500 K.

Received 10th July 2018,
Accepted 13th August 2018

DOI: 10.1039/c8cp04332a

rsc.li/pccp

1. Introduction

Boron as an electron-deficient element possesses new chemistry[1–6] that differs from carbon, its nearest neighbor in the periodic table. Boron-based nanoclusters[4,7–15] are of current interest in physical chemistry and materials science. Elemental boron clusters assume planar or quasi-planar (2D) geometries in a wide range of sizes, up to 40 atoms for anions,[4] which are governed by aromaticity, antiaromaticity, or conflicting aromaticity.[5] Planar boron clusters also show an isolobal analogy to boranes and hydrocarbons in terms of chemical bonding.[5,9,10] These 2D clusters are dominated by close-packing triangular B_3 units, which are complemented by quadrangular, pentagonal, and hexagonal defect holes.

Notably, monocyclic boron rings are scarce in 2D boron clusters,[5,7,9,10] nor do they appear in low-dimensional boron nanomaterials (such as borospherenes,[4] nanotubes,[16] and borophenes[2,3]). In contrast, boron double chains (BDCs) or BDC ribbons[4,14] prevail in low-dimensional boron systems, which help compensate for electron-deficiency. Carbon clusters are known to form monocyclic ring structures, with C_{10} being a typical example.[17,18] Thus, it is of interest to raise a couple of fundamental questions. Is it possible to make or stabilize monocyclic boron rings in gas-phase boron clusters? Can we chemically convert boron into carbon (or can we design a boron cluster that resembles a carbon one)? If yes, how? What is the nature of bonding in such monocyclic boron rings? What are the possible electron counting rules?

Considering the intrinsic electron deficiency of boron, a natural way to approach the above mentioned goal is to pour a sufficient number of extra electrons into a boron cluster. To this end, binary Be–B clusters are ideal systems, in which Be has a rather low electronegativity and is capable of donating up to two electrons per Be atom. Such binary clusters have been explored recently.[19–21] In particular, Zhai and coworkers studied a $Be_6B_{11}^-$ cluster, unraveling two highly competitive 3D isomeric structures: a boron helix *versus* a boron-based sandwich.[11]

[a] *Nanocluster Laboratory, Institute of Molecular Science, Shanxi University, Taiyuan 030006, China. E-mail: hj.zhai@sxu.edu.cn*
[b] *Department of Chemistry, Xinzhou Teachers University, Xinzhou 034000, Shanxi, China*

† Electronic supplementary information (ESI) available: Orbital composition analysis for the $Be_6B_{10}^{2-}$ cluster (Table S1); optimized structure of the salt complex $Be_6B_{10}Na_2$ cluster at PBE0 (Fig. S1); an alternative AdNDP scheme for delocalized π/σ frameworks of $Be_6B_{10}^{2-}$ (Fig. S2); AdNDP bonding pattern of the C_{10} cluster (Fig. S3); CMOs and AdNDP data of the TS structure of $Be_6B_{10}^{2-}$ (Fig. S4 and S5); and displacement vectors of selected vibrational frequencies of $Be_6B_{10}^{2-}$ cluster and two TS structures (Fig. S6). See DOI: 10.1039/c8cp04332a

The latter species possesses structural fluxionality with dual dynamic modes. Fluxional clusters[8,11,22–31] are intriguing in physical chemistry as well as in nanoscience and nanotechnologies. Boron is the magic element for structural fluxionality. Previous fluxional clusters are rare and they have only one dynamic mode, either as molecular Wankel motors[8,22,23] or subnanoscale tank treads.[13,28]

The B_{10} cluster is quasi-planar[10] and features close-packed boron triangles, which have no rhombic or rectangular defect sites. The shape is anticipated to be dynamically nonfluxional. Indeed, a recent theoretical work[27] suggests that B_{10} has a considerable energy barrier for in-plane rotation (12.7 kcal mol^{-1} at PBE0). We will show herein that upon alloying with Be in a binary $Be_6B_{10}^{2-}$ cluster, a few notable changes take place. Firstly, the 2D close-packed B_{10} cluster turns into a monocyclic ring, which becomes part of a well-defined global-minimum (GM) $Be_6B_{10}^{2-}$ cluster. Second, the B_{10} cluster maintains its chemical integrity in the alloy, except that it is now in a charged state of $[B_{10}]^{10-}$ owing to electron transfer from Be centers. Third, the alloy cluster system is dynamically fluxional with two dynamic modes, for which the B_{10} ring is structurally robust at least up to 1500 K. Fourth, the present data demonstrate an idea of electronic transmutation,[32–37] where a B^- is chemically converted to a C and a $[B_{10}]^{10-}$ cluster closely resembles a C_{10} cluster in terms of geometry and bonding. Note that the C_{10} cluster[17] itself is considered to mark a chain-to-ring structural transition in carbon clusters, whose ring structure has unusual stability because it conforms to the Hückel rule for aromaticity.

2. Methods

Global structural searches were conducted for $Be_6B_{10}^{2-}$ cluster using unbiased Coalescence Kick (CK)[38–40] and Minima Hopping (MH)[41,42] algorithms. Some 8000 stationary points in total were probed on the potential energy surface. Subsequently, candidate low-lying isomers were re-optimized at the PBE0/6-311+G(d) level,[43] with zero-point energy (ZPE) corrections. Frequency calculations were done at the same level to confirm that the reported structures are true minima unless stated otherwise. To confirm the energetics, the top-five low-lying isomers were benchmarked using single-point CCSD(T) calculations,[44–46] that is, at the CCSD(T)/6-311+G(d)//PBE0/6-311+G(d) level.

To evaluate the energy barrier with regards to molecular dynamics (MD) and for comparison with the literature,[11] the GM and transition state (TS) structures of $Be_6B_{10}^{2-}$ were also optimized at the PBE0-D3/def2-TZVP level along with the frequency calculations. QST2 and intrinsic reaction coordinate (IRC) calculations were performed at the PBE0/6-311+G(d) level to locate and confirm TS structures. Salt complex cluster $Be_6B_{10}Na_2$ was also optimized at the PBE0/6-311+G(d) and PBE0-D3/def2-TZVP levels.

Chemical bonding was elucidated using canonical molecular orbitals (CMOs), adaptive natural density partitioning (AdNDP),[47] and natural bond orbital (NBO) analysis[48] at the PBE0/6-311+G(d) level; the latter offers Wiberg bond indices (WBIs). Nature charges were calculated independently using NBO 6.0.[49] Orbital composition was analyzed by the Multiwfn program.[50] Nucleus-independent chemical shifts (NICSs)[51] were calculated for selected species at the PBE0/6-311+G(d) level to assess aromaticity. Born–Oppenheimer molecular dynamics (BOMD) simulations were performed using CP2K.[52] AdNDP results were visualized using Molekel 5.4.[53] All electronic structure calculations were performed using the Gaussian 09 package.[54]

3. Results

3.1. Global-minimum $Be_6B_{10}^{2-}$ cluster

Our computer global searches, PBE0/6-311+G(d) calculations, and CCSD(T) benchmarking lead to the GM structure of the $Be_6B_{10}^{2-}$ cluster: **1** (C_{2v}, $^1A_1$). Overall, cluster **1** is reasonably well defined on the potential energy surface (**1–20**; Fig. 1–5), being about 10 kcal mol^{-1} more stable than its nearest competitor at both the PBE0 and single-point CCSD(T) levels. Cluster **1** consists of three coaxial rings: a monocyclic B_{10} ring in the middle and two Be_3 rings at the top and bottom (Fig. 2(a)). The two Be_3 rings overlap spatially, forming a trigonal prism with distortion (Fig. 2(b)). Interlayer bonding between Be_3 rings is minimal despite their closeness in space (*vide infra*), which justifies the assessment of cluster **1** as a sandwich.

The nature of B–B, Be–Be, and B–Be bonding in cluster **1** can be largely recognized from their bond distances. Recommended covalent radii by Pyykkö[55] give the upper limit of single B–B, double B=B, and single Be–Be bonds as 1.70, 1.56, and 2.04 Å, respectively. For further reference, a typical B=B double bond is 1.51 Å,[56–58] whereas the bond distances in Be_2 and Be_2^+ are 2.44 Å (van der Waals) and 2.21 Å (half bond), respectively.[59] Therefore, the B–B bonds in the B_{10} ring of cluster **1** (1.55–1.60 Å) are beyond single bonds, with clear double bond characters.

The Be–Be links in Be_3 rings (2.06–2.14 Å) indicate strong bonding, probably comparable to that in Be_2^+. Interlayer Be–Be distances (2.11–2.24 Å) are also short, but their WBIs are close to zero (Fig. 3(a)), suggesting that there is no bonding. Between the Be_6 core and outer B_{10} ring, the Be–B links as depicted in Fig. 2(b) are diverse, spanning from 1.84 to 2.20 Å (not shown). Such bonds are quite ionic, with a rather weak covalent component.

5w?>One may argue that a dianion cluster such as **1** is electronically unstable, due to Coulomb repulsion between the two extra charges. Thus we also explored the neutral salt complex, $Be_6B_{10}Na_2$, using two Na^+ counter-ions to balance charges. Among different configurations, the lowest-energy one is a C_{2v} ($^1A_1$) salt complex; see the ESI,† (Fig. S1). It is a true minimum, showing virtually identical geometry with respect to GM cluster **1**. This structure was also optimized at the PBE0-D3/def2-TZVP level (not shown), resulting in similar geometry.

3.2. Selected isomeric and transition-state structures

Higher energy isomers of the $Be_6B_{10}^{2-}$ cluster (Fig. 1) are generally unimportant in light of the reasonably defined GM **1** (C_{2v}, $^1A_1$) cluster. We choose to briefly describe isomers **3** and **8** only. Isomer **3** as a local minimum (LM) differs from GM **1** by a twist of one Be_3 ring against another, so that two Be_3 rings are

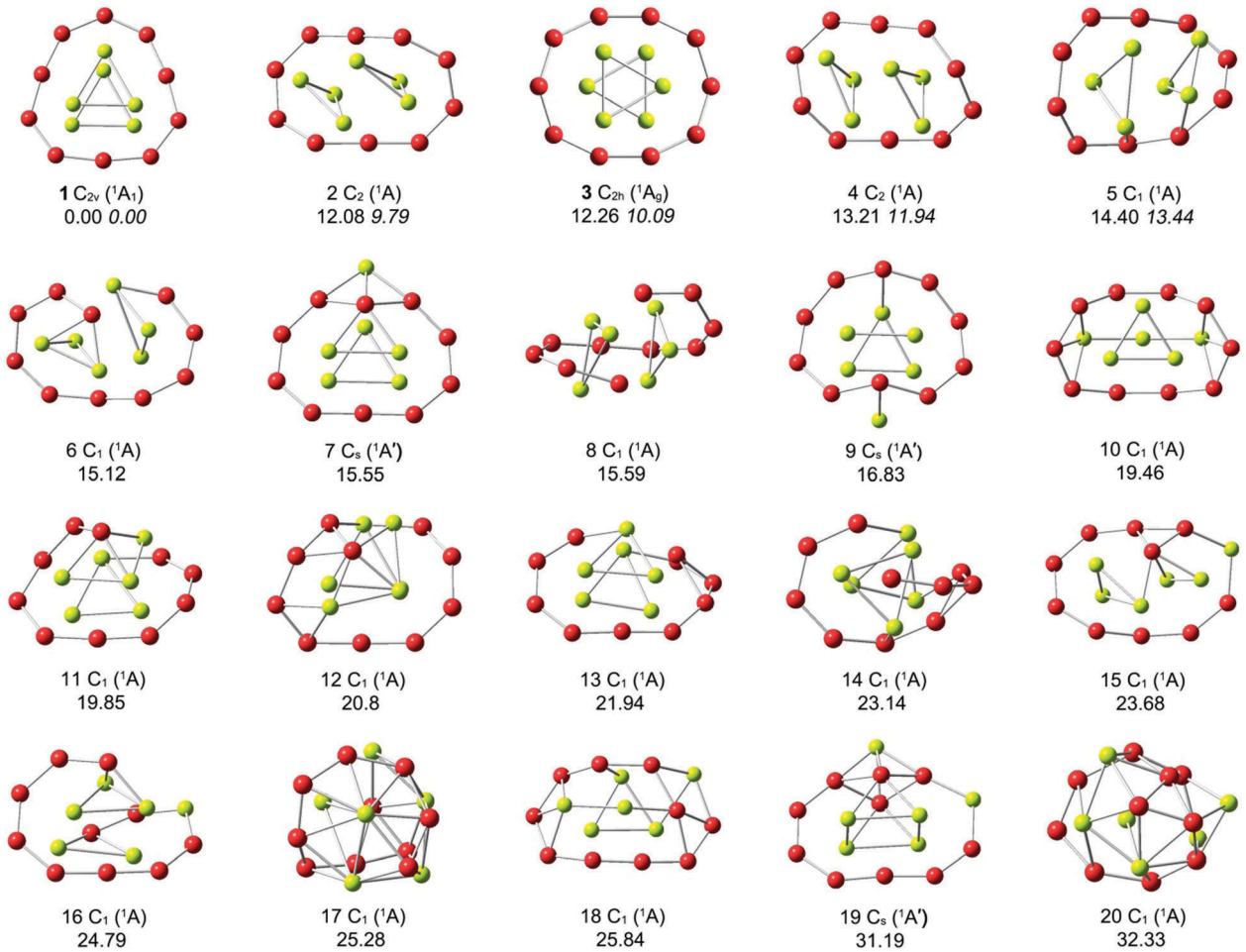

Fig. 1 Alternative optimized low-lying isomeric structures of the $Be_6B_{10}^{2-}$ cluster at the PBE0/6-311+G(d) level. Relative energies are given in kcal mol^{-1} at PBE0 with zero-point energy (ZPE) corrections, as well as at a single-point CCSD(T) level (in italic) for the top five lowest-lying isomers.

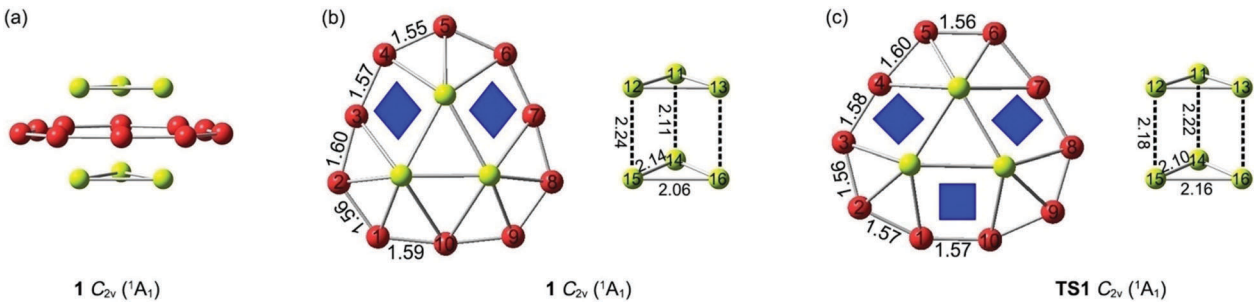

Fig. 2 The optimized global-minimum (GM) structure of (a) the $Be_6B_{10}^{2-}$ (**1**, C_{2v}, $^1A_1$) cluster at the PBE0/6-311+G(d) level. (b) The top-view of cluster **1** and side-view of its prismatic Be_6 core. (c) The optimized transition state (TS) structure of $Be_6B_{10}^{2-}$, **TS1** (C_{2v}, $^1A_1$). Bond distances are labeled in Å. The B atoms are shown in red and Be in yellow.

in a staggered fashion (Fig. 4 and 5). The energy cost is ~10 kcal mol^{-1} at single-point CCSD(T). The B–B distances (1.57–1.63 Å) in **3** expand slightly as compared to GM **1**, while those of Be–Be (2.06–2.10 Å) shrink slightly. These minor changes reflect the spatial constraints for rotation between two Be_3 rings. Isomer **8** contains an open, helix B_{10} chain. It is ~15 kcal mol^{-1} above GM **1**, in contrast to our recent report on a $Be_6B_{11}^-$ cluster,[11] for which the helix isomer is energetically competitive with the sandwich cluster. Thus, chain size has a remarkable effect on the stability of a boron helix. While exploring the potential energy surface of the $Be_6B_{10}^{2-}$ cluster, we also located certain TS structures: **TS1** and **TS2** (Fig. 2(c) and 4(b)).[60]

3.3. Wiberg bond indices and natural charges

The above analyses based on the geometries unveil a rough bonding picture for the $Be_6B_{10}^{2-}$ cluster. NBO analysis confirms

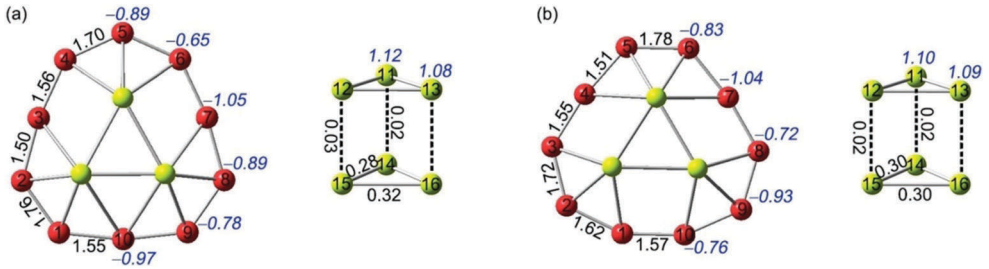

Fig. 3 Calculated Wiberg bond indices (WBIs; in black) and natural atomic charges (in |e|; blue) at the PBE0/6-311+G(d) level. (a) GM $Be_6B_{10}^{2-}$ (**1**). (b) TS structure (**TS1**).

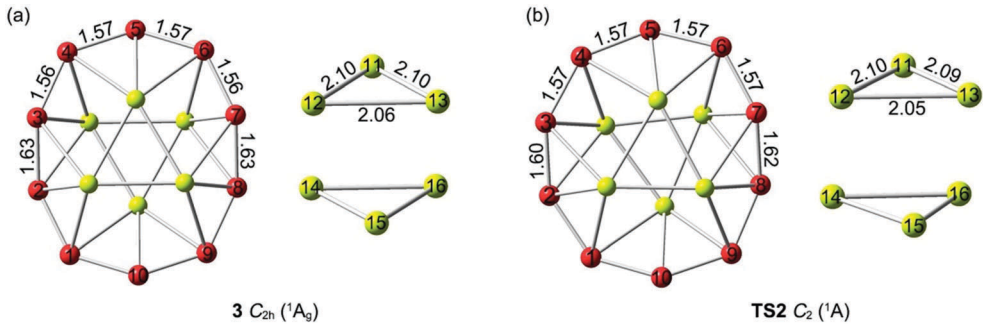

Fig. 4 The local minimum (LM) structure of (a) $Be_6B_{10}^{2-}$ (**3**, C_{2h}, ^1A_g) at the PBE0/6-311+G(d) level and (b) TS structure **TS2** (C_2, ^1A). Bond distances are labeled in Å. The B atoms are shown in red and Be in yellow.

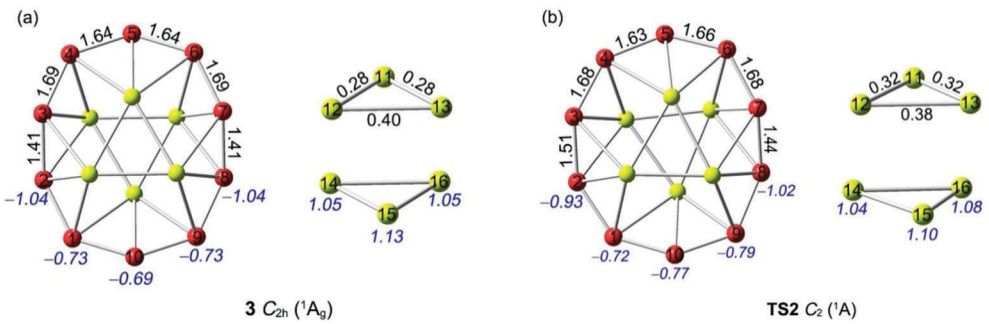

Fig. 5 Calculated WBIs (in black) and natural atomic charges (in |e|; blue) at the PBE0/6-311+G(d) level. (a) LM $Be_6B_{10}^{2-}$ (**3**). (b) **TS2**.

this picture, using WBIs and natural atomic charges. Calculated WBI values for B–B links in the GM cluster **1** are 1.50–1.76 (Fig. 3(a)), which are well beyond single bonds, suggesting delocalized bonding in the outer B_{10} ring. The WBIs of Be_3 rings are 0.28/0.32, hinting at a delocalized bonding system here. In contrast, the WBIs of interlayer Be–Be links are negligibly small (0.02/0.03). There is no interaction between two Be_3 rings. The WBI data are in line with a triple-layered sandwich cluster **1**, whose two Be_3 rings are independent from each other.

Natural atomic charges in GM **1** indicate substantial interlayer charge transfers from the two Be_3 rings to the middle B_{10} layer. Each Be center carries a positive charge of greater than 1.0, and six Be atoms collectively donate a net charge of 6.56 |*e*| to the B_{10} ring. The formal number of charges is anticipated to be even larger, resulting in a highly charged cluster system. NBO data for **TS1** are similar to those of GM **1**, except that the charges shift circularly with the Be centers (Fig. 3(b)). Charge transfers from Be to B in the system are rather local processes, depending sensitively on coordination with the Be centers.

4. Discussion

4.1. Chemical bonding in the sandwich $Be_6B_{10}^{2-}$ cluster: four-fold π/σ aromaticity

It is relatively straightforward to elucidate the bonding in GM $Be_6B_{10}^{2-}$ (**1**, C_{2v}, $^1A_1$) cluster through CMO analyses. Cluster **1** is a bonding system with 44 valence electrons, which occupy 22 CMOs as depicted in Fig. 6. Here the CMOs are sorted into five subsets, according to the type of atomic orbital (AO) of which a specific CMO is composed. Subset (a) involves 10 CMOs, mainly derived from B 2s AOs in the outer B_{10} ring. The CMOs have 0, 1, 2, 3, 4, and 5 nodal planes, respectively, following the

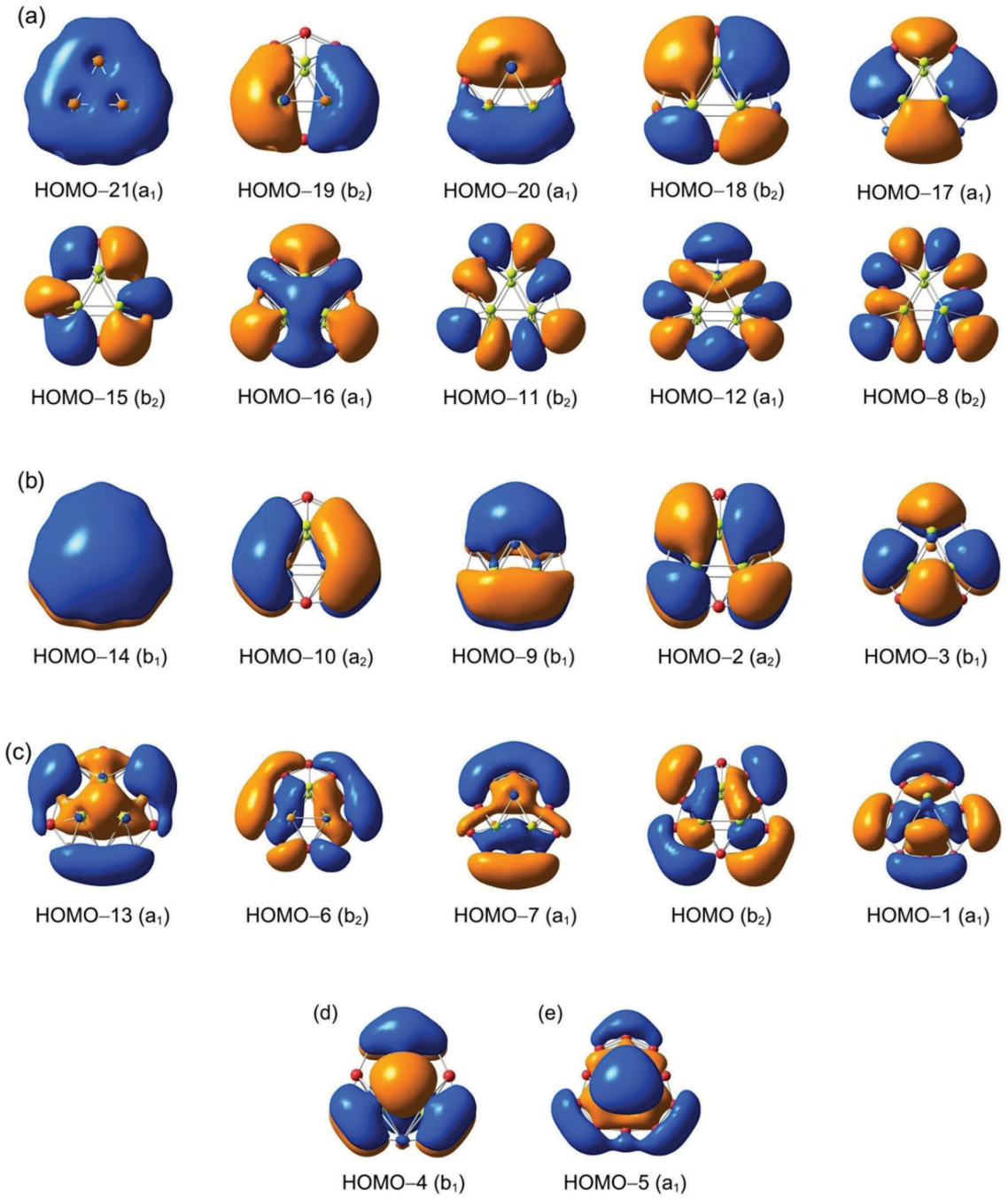

Fig. 6 Pictures of canonical molecular orbitals (CMOs) of the GM $Be_6B_{10}^{2-}$ (**1**) cluster. (a) Ten CMOs for classical B–B σ single bonds in the outer B_{10} ring. (b) Five delocalized π CMOs. (c) Five delocalized σ CMOs. (d) One delocalized "π" CMO, dominated by the two Be_3 rings of the prismatic Be_6 core. (e) One delocalized σ CMO with major contribution from the two Be_3 rings.

construction principles. They represent a complete series of CMOs that are responsible for peripheral B–B σ bonding in the B_{10} ring, which can be transformed to and localized as two-center two-electron (2c–2e) Lewis B–B σ bonds, one for each B–B link. This subset is the only Lewis element in cluster **1**, consuming 20 electrons. All of the other 24 electrons participate in delocalized bonding.

Subset (b) contains five π CMOs, which are derived primarily from B $2p_z$ AOs; see Table S1 (ESI†) for their orbital components. Among these, HOMO−14 has the largest contribution from the Be_6 prism (38.1%), which can recombine constructively/destructively with HOMO−4 to fully recover two spatially separated "π" CMOs: one for the outer B_{10} ring and the other for the inner Be_6 prism. Subset (b) also strictly follows the building principles, with 0, 1, and 2 nodal planes that are perpendicular to the B_{10} ring; the intrinsic nodal plane associated with the p-type AO is not counted, as routine. Indeed, these CMOs show one-to-one correspondence, in terms of the spatial pattern, to the lower

energy CMOs in subset (a). The five π CMOs cannot be localized and represent a 10π aromatic subsystem, conforming to the $(4n + 2)$ Hückel rule. Subset (c) is analogous to subset (b), except that the former is σ in nature based on radial B 2p AOs. These 10σ electrons cannot be transformed into Lewis bonds and render σ aromaticity to cluster **1**.

Subsets (d) and (e) are mainly clouded on the inner Be_6 prism, which can be fully "purified" upon combination with HOMO−14 and HOMO−13, respectively, as mentioned earlier. The two "purified" bonds represent a constructive/destructive combination between two Be_3 rings, which are readily transformed to two 3c–2e σ bonds, one on each Be_3 ring. Thus a Be_3 ring in cluster **1** is held together merely by one 3c–2e σ bond.

In short, the sandwich cluster features four-fold electron delocalization: the B_{10} ring has 10π and 10σ subsystems and each Be_3 ring has a 2σ subsystem, which all satisfy the Hückel rule, rendering four-fold π/σ aromaticity for cluster **1**. This bonding picture is beautifully borne out using AdNDP (Fig. 7). An alternative AdNDP scheme for 10π/10σ subsystems is presented in Fig. S2 (ESI†).[61] Since each Be_3 ring has only one 3c–2e σ bond, cluster **1** should be formally formulated as $[Be_3]^{4+}[B_{10}]^{10-}[Be_3]^{4+}$, a highly-charged electron-transfer complex. Indeed, NBO analysis gives an effective formula of $[Be_3]^{3.28+}[B_{10}]^{8.56-}[Be_3]^{3.28+}$ (Fig. 3(a)). One reviewer suggests an interesting possibility of applying charge decomposition analysis (CDA)[62] to this charge transfer complex. While we are aware of the fact that CDA is a partitioning scheme for donor–acceptor interactions and applies best for metal–ligand systems, we chose to accommodate the reviewer and ran preliminary CDA calculations. The results are in line with a charge-transfer complex.[63] We stress that the bonding picture is entirely reached *via* CMO analyses, further confirmed by AdNDP and NBO data. With this picture, cluster **1** is held together primarily *via* electrostatics between the three layers, with secondary haptic covalent bonds. The latter have WBI values of 0.11–0.16.

Interestingly, the two Be_3 rings, which have 2s electrons only, participate in both π and σ bonding with the B_{10} ring. Their main CMOs are HOMO−14/HOMO−4 and HOMO−13/HOMO−5 (Fig. 6). The shape of HOMO−14 is peculiar. Two layers of Be_3 3c–2e σ clouds couple out-of-phase and disguise as a "π" component, facilitating a global π bond. The B $2p_z$ component serves as a clamp (with intrinsic thickness) and pulls the two Be_3 rings close, balanced by electrostatics between the $Be_3/B_{10}/Be_3$ rings. Here the Be_3–Be_3 bonding is not necessarily optimal despite short interlayer Be–Be distances, leading to an unusual situation: close and nonbonding.

NICS calculations may be used as a qualitative measure for aromaticity of a molecular system. Generally, $NICS_{zz}$ is considered as a better indicator for planar molecules. The calculated $NICS_{zz}$ values at the PBE0/6-311+G(d) level are highly negative for cluster **1**: −77.78 ppm at the center of the B_{10} ring and −66.01 ppm at 1 Å

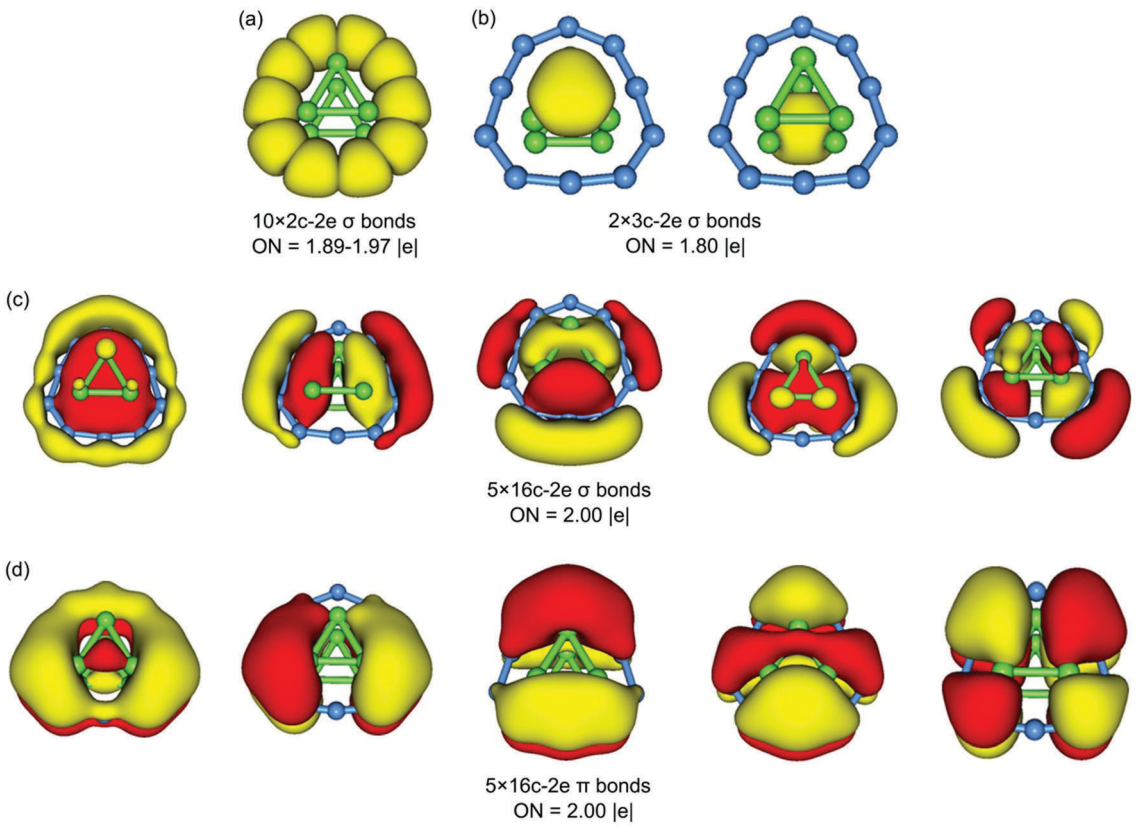

Fig. 7 The bonding pattern of the GM $Be_6B_{10}^{2-}$ (**1**) cluster *via* adaptive natural density partitioning (AdNDP) analysis. Occupation numbers (ONs) are shown.

Table 1 Nucleus-independent chemical shifts (NICS; in ppm) for the $Be_6B_{10}^{2-}$ (**1**, C_{2v}, $^1A_1$) cluster. $NICS_{zz}(0)$ and $NICS_{zz}(1)$ are calculated at the center of the B_{10} ring and at 1 Å above the ring center, respectively. Also presented for comparison are NICS data of D_{5h} C_{10} and D_{10h} $C_{10}H_{10}$

Species	$Be_6B_{10}^{2-}$ (**1**)	D_{5h} C_{10}	D_{10h} $C_{10}H_{10}$
$NICS_{zz}(0)$	−77.78	−71.06	−39.20
$NICS_{zz}(1)$	−66.01	−57.82	−37.47

above the center (Table 1), which confirm the assessment of π/σ aromaticity, in line with CMO and AdNDP analyses. It should be stressed that the $NICS_{zz}$ values herein are the collective effects of all four-fold π/σ aromatic subsystems to a probing point, so that $NICS_{zz}(1)$ is not solely associated with π aromaticity of the B_{10} ring, because of the "perturbation" of σ aromaticity of the Be_3 ring in the vicinity. Indeed, we do not intend to disentangle the contributions of the four aromatic subsystems from each other. The NICS data serve only as an additional support of π/σ aromaticity in the $Be_6B_{10}^{2-}$ (**1**) cluster, which is a relatively minor issue of this paper.

4.2. Electronic transmutation: analogy between the $Be_6B_{10}^{2-}$ cluster, the carbon cluster C_{10}, and the hydrocarbon compound $C_{10}H_{10}$

CMO and AdNDP analyses show that **1** is a charge transfer complex: $[Be_3]^{4+}[B_{10}]^{10-}[Be_3]^{4+}$. Specifically, "antibonding" electrons from Be_3 rings are transferred to "bonding" CMOs of the B_{10} ring. Charge-transfer not only helps compensate for boron's electron-deficiency, but also strengthens bonding in the Be_3 rings. The resultant complex cluster **1** has a sandwich shape with aromatic $[Be_3]^{4+}/[B_{10}]^{10-}/[Be_3]^{4+}$ subsystems, which are held together through electrostatics.

In contrast to carbon, bare boron clusters do not form monocyclic rings. The B_{10} cluster is quasi-planar with two dovetailed hexagonal pyramids, which is composed solely of close-packing B_3 triangles.[10] It has delocalized 6π and 8σ subsystems, clouding on the 2D surface. On the other hand, the C_{10} cluster has monocyclic geometry.[17] Thus, it seems feasible that if a sufficient number of extra electrons are donated to the B_{10} cluster, the latter can be transformed from a close-packed 2D sheet to a monocyclic ring (akin to C_{10}). This is exactly what happens for the B_{10} ring in cluster **1**.

The delocalized π/σ bonding of the $[B_{10}]^{10-}$ ring in cluster **1** may be compared to those of its carbon-based analogs: hydrocarbon compound D_{10h} $C_{10}H_{10}$ and carbon cluster D_{10h} C_{10}. Note that the C_{10} cluster[17,64] adopts a monocyclic D_{5h} structure; D_{10h} is a second-order saddle point at the PBE0/6-311+G(d) level. Likewise, D_{10h} $C_{10}H_{10}$ is a model system. As shown in Fig. 8, the 10π systems in the three species are identical, whereas the 10σ system in D_{10h} C_{10} also resembles that in $[B_{10}]^{10-}$. AdNDP analysis can also fully reproduce the 10π/10σ aromatic system in D_{10h} C_{10} (Fig. S3, ESI†). The above comparison renders the sandwich $Be_6B_{10}^{2-}$ cluster an analog of D_{10h} C_{10} and D_{10h} $C_{10}H_{10}$. In fact, $[B_{10}]^{10-}$ is isoelectronic to C_{10}. Thus, cluster **1** suggests the possibility of stabilizing monocyclic boron rings *via* charge donation. Alternatively, it is an example of electronic transmutation,[32–37] in which B^- is chemically converted to C in terms of cluster structure and chemical bonding.

4.3. Dynamic fluxionality of the $Be_6B_{10}^{2-}$ cluster

The sandwich $Be_6B_{10}^{2-}$ (**1**) cluster resembles the $Be_6B_{11}^-$ cluster[11] in terms of geometry; the dynamic fluxionality of the latter was reported recently by our group. The $Be_6B_{10}^{2-}$ cluster serves to address a couple of critical issues. Firstly, to demonstrate the idea that sandwich clusters can become energetically competitive in binary Be–B systems. Note that the $Be_6B_{10}^{2-}$ (**1**) cluster is well defined as GM, whereas the prior $Be_6B_{11}^-$ cluster has a competitive helix *versus* sandwich isomers. Second, to demonstrate electronic transmutation[32–37] using analogy between $[B_{10}]^{10-}$ and C_{10}. They not only adopt similar structures, but also have similar bonding (two-fold 10π/10σ aromaticity). This concept suggests further opportunities are available to stabilize monocyclic boron rings in charge transfer clusters. We believe that the strategy may be explored in synthetic works and should lead to unconventional boron compounds. Third, to examine factors that affect structural fluxionality and energy barriers in dynamic cluster systems, as detailed below.

During the global structural searches, we have identified GM cluster **1**, LM **3**, and two TS structures (**TS1** and **TS2**) for the $Be_6B_{10}^{2-}$ cluster, where TS structures were obtained and confirmed with the aid of QST2 and IRC calculations. The relationship between these structures is outlined in Fig. 9. As an example, chemical bonding in **TS1** is analyzed using CMOs and AdNDP (Fig. S4 and S5, ESI†), which is quite similar to GM **1**. With the above key structures, it is natural to ask a number of questions. Is the $Be_6B_{10}^{2-}$ cluster dynamically fluxional? Can more than one modes be present in the $Be_6B_{10}^{2-}$ cluster? How are its dynamic properties different from the prior $Be_6B_{11}^-$ cluster? What determines the energy barriers, in particular for twisting between the two Be_3 rings?

Let us start with GM cluster **1**. It has rhombic structural "defects" (Fig. 2(b)),[11,13] which are the most flexible portion in the system and can facilitate rhombic-to-square transformation and *vice versa*. Vibrational analyses indicate that cluster **1** has at least three frequencies relevant to intramolecular rotation: 148.0, 133.9 and 542.4 cm^{-1} at the PBE0/6-311+G(d) level (Fig. S6, ESI†). For the 148.0 cm^{-1} frequency, the two Be_3 rings move in phase, countering the direction of the outer B_{10} ring. Thus, Be_6 remains as a prism and the B_{10} ring rotates around the prism. Such a movement deforms the rhombic defects in **1** and naturally leads to **TS1**, whose imaginary frequency (100.1i cm^{-1}; Fig. S6(b), ESI†) is also in line with in-plane rotation. The 133.9 and 542.4 cm^{-1} frequencies of cluster **1** feature counter-rotation (that is, twisting) between the two Be_3 rings; the latter frequency probably suggests a higher energy barrier. The twisting movement leads to **TS2**, which has an imaginary frequency of 132.2i cm^{-1}. In summary, cluster **1** can in principle move in two dynamic modes, revolution (orbiting) *versus* rotation (twisting).

Quantitatively, the revolution barrier of cluster **1** is calculated to be 0.30 kcal mol^{-1} at the PBE0/6-311+G(d) level, which is refined to 0.36 and 0.81 kcal mol^{-1} at the PBE0-D3/def2-TZVP and CCSD(T)/def2-TZVP levels, respectively. This barrier is minor,

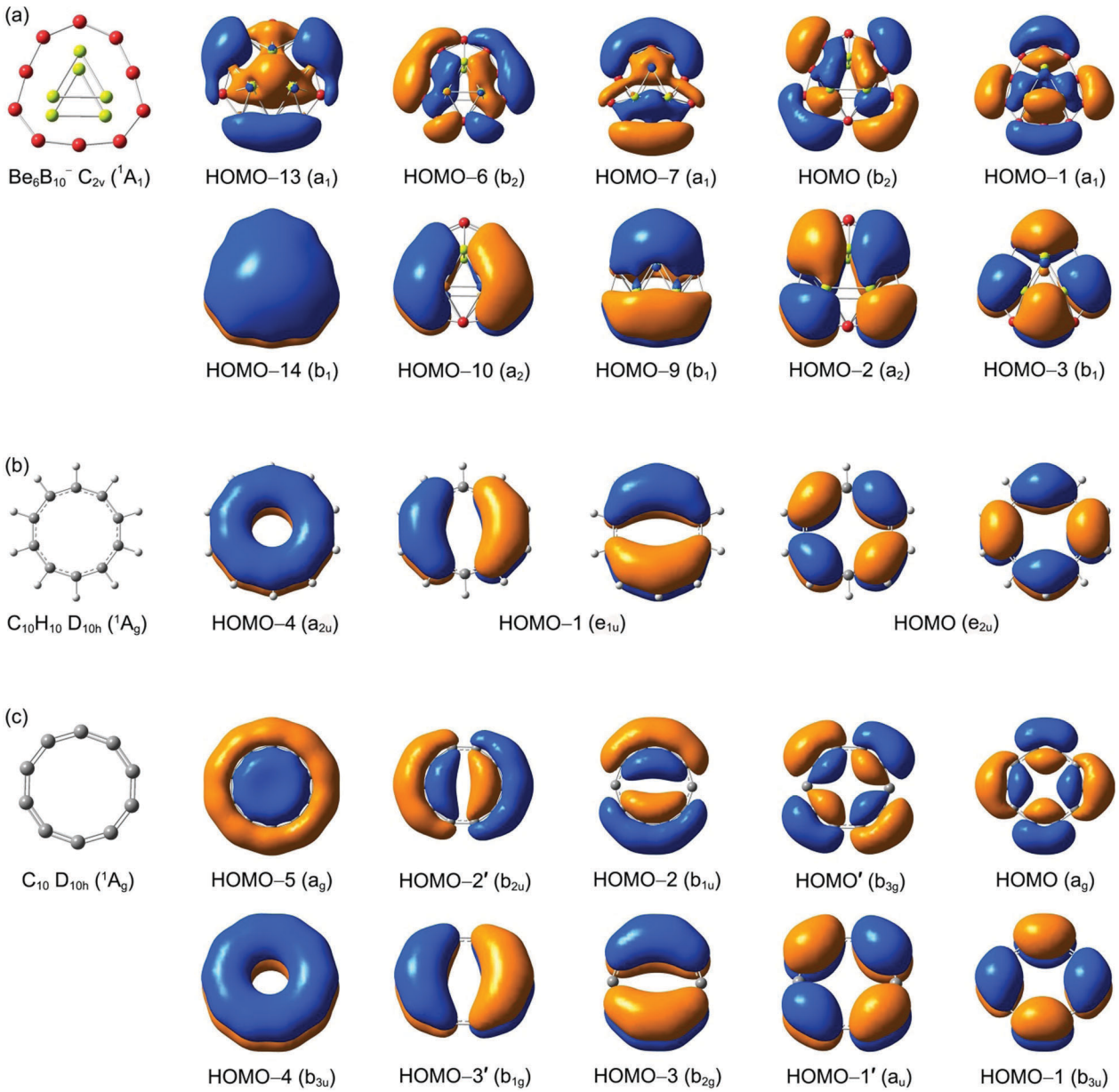

Fig. 8 Comparison of (a) delocalized π/σ CMOs of the GM $Be_6B_{10}^{2-}$ (**1**) cluster with those of (b) D_{10h} $C_{10}H_{10}$ and (c) D_{10h} C_{10}. The latter two are model clusters only.

suggesting that the B_{10} ring in **1** is likely to orbit freely at moderate temperatures. Furthermore, the energy barrier for the twisting mode is calculated to be 12.56 and 12.69 kcal mol^{-1} at the PBE0/6-311+G(d) and CCSD(T)/def2-TZVP levels, respectively. We also performed PBE0-D3/def2-TZVP calculations and the barrier is calculated to be 12.95 kcal mol^{-1}. The twisting barrier is quite high in comparison to 4.52 kcal mol^{-1} for the prior $Be_6B_{11}^-$ cluster,[11] hinting that cluster **1** can twist only at very high temperatures.

We believe that the difference between cluster **1** and $Be_6B_{11}^-$ in revolution/rotation barriers is due to subtle geometric reasons. The B_{10} ring in cluster **1** is only marginally smaller than the B_{11} ring in $Be_6B_{11}^-$, with a width/height of 4.81/5.05 Å for the former *versus* 4.94/5.31 Å for the latter. Such a tiny reduction of the ring size in cluster **1** would reinforce the confinement of the Be_6 prism, alter Be–B bonding as well as Be_3–B_{10} and Be_3–Be_3 interactions, and affect the dynamic barriers (in particular for the twisting mode). Specifically, the peripheral B–B distances in cluster **1** (Fig. 2(b)) are slightly longer than those in $Be_6B_{11}^-$ (Fig. S1(b), ESI†), by 0.04 Å in average. However, the Be_3 rings in cluster **1** are more compact (by at least 0.1 Å). These parameters hint at discernible geometric constraints in cluster **1**. In other words, the outer B_{10} ring in cluster **1** seems a bit too small and the inner Be_3 rings are too large, which are not a perfect match for dynamics and should result in elevated barriers.[65] Ideally, a system with slightly too large an outer ring and too small an inner

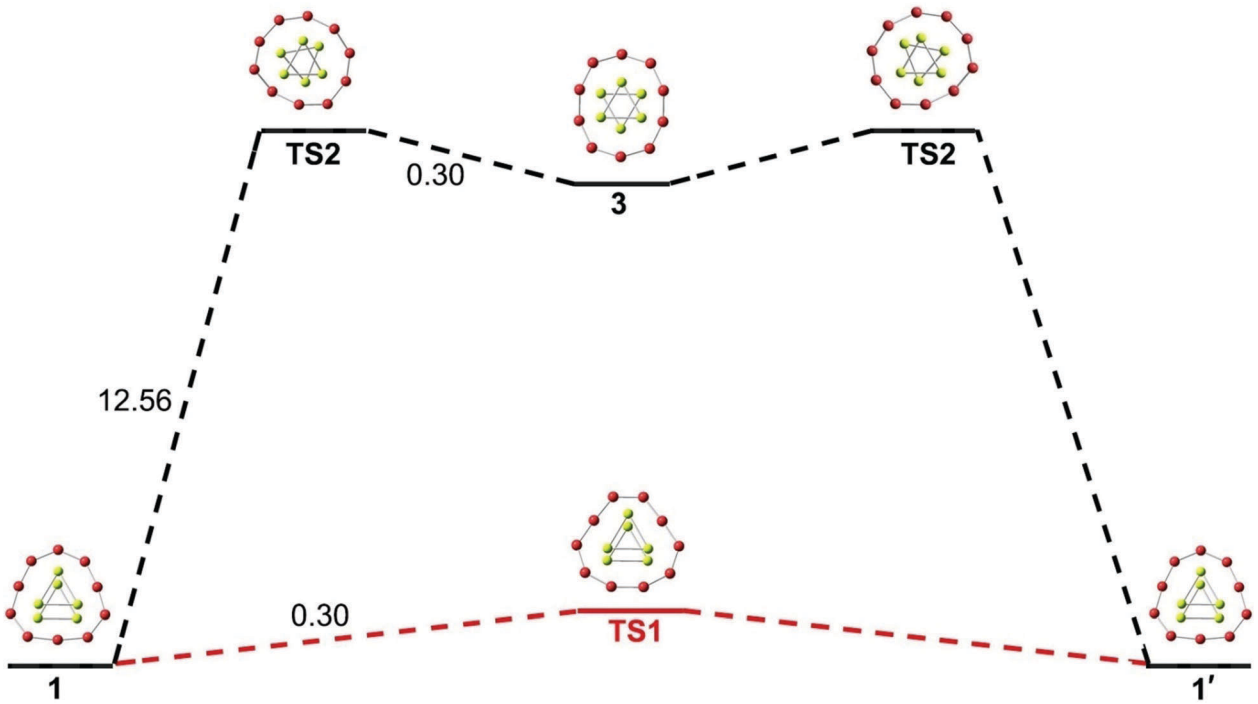

Fig. 9 Energy pathways for two dynamic modes of the $Be_6B_{10}^{2-}$ (**1**) cluster. The revolution of the outer B_{10} ring around the prismatic Be_6 core (bottom curve, in red) takes place directly *via* **TS1**, with a minor energy barrier of 0.30 kcal mol^{-1} at the PBE0/6-311+G(d) level. The rotation dynamics (twisting) between the two Be_3 rings (upper curve), proceeds through the LM structure **3** and involves two isoenergetic TS structures (**TS2**). The energy barrier for **GM1–TS2** is 12.56 kcal mol^{-1} and the energy difference for **3–TS2** is 0.30 kcal mol^{-1}.

core may benefit dynamic fluxionality, because it dilutes the bonding between the outer ring and the inner core. This understanding shall benefit forthcoming rational design or discovery of dynamic systems with optimal dual-mode fluxionality.

To demonstrate dual-mode dynamic fluxionality of sandwich cluster **1**, we performed BOMD simulations at different temperatures. Typical simulations are presented in the form of short movies (300, 600, and 1500 K; see ESI†), which were carried out for 20 ps using the CP2K package at the PBE0/DZVP-GTH level. Initial conditions were chosen to correspond to the microcanonocal ensemble (*NVE*). At room temperature (300 K), the Be_6 prism in cluster **1** only jitters back and forth around its equilibrium position and the cluster never reaches the **TS1** structure. Neither revolution (orbiting) nor rotation (twisting) is activated at this temperature.

At 600 K, the B_{10} ring can glide freely around the Be_6 prism, like a flexible chain, and the inner Be_3 rings only jitter around their equilibrium positions. No twisting event occurs and the Be_6 prism maintains it's integrity. Similar dynamics is observed at 1000 K and 1200 K, indicating that the twisting mode remains inactive. At a high temperature of 1500 K, both dynamic modes are functioning: the outer B_{10} ring glides like a hula hoop, whereas the two Be_3 rings also twist occasionally against each other akin to dancing the tango. Alternatively, dual dynamic modes of revolution/rotation make an earth-moon system at the subnanometer scale. It is remarkable that the B_{10} and the Be_3 rings in cluster **1** are robust against fragmentation at a temperature as high as 1500 K, which may be ascribed to multifold π/σ aromaticity in the system.

5. Conclusions

We report on computational design of a coaxial triple-layered $Be_6B_{10}^{2-}$ sandwich cluster, which is established as the global minimum of the system *via* machine searches and quantum chemical calculations. It features a monocyclic B_{10} ring, sandwiched by two Be_3 rings on top and underneath. The latter two rings form a trigonal-prism albeit without interlayer Be–Be bonding. The B_{10} ring in the $Be_6B_{10}^{2-}$ cluster differs fundamentally from the free B_{10} cluster, and yet it resembles a C_{10} cluster closely. Bonding analyses show that the $Be_6B_{10}^{2-}$ cluster possesses four-fold π/σ aromaticity: 10π and 10σ delocalization for the B_{10} ring and 2σ delocalization for each Be_3 ring. The bonding picture indicates that $Be_6B_{10}^{2-}$ is a charge transfer complex with a formula of $[Be_3]^{4+}[B_{10}]^{10-}[Be_3]^{4+}$. The highly charged $[B_{10}]^{10-}$ ring is chemically converted to a C_{10} cluster *via* "electronic transmutation", which underlies the monocyclic boron ring in the $Be_6B_{10}^{2-}$ cluster. Indeed, the $[B_{10}]^{10-}$ and C_{10} species are similar in geometry and bonding, including two-fold π/σ aromaticity. Lastly, the sandwich $Be_6B_{10}^{2-}$ cluster has dynamic structural fluxionality, featuring two dynamic modes. The B_{10} ring is robust against rupture or fragmentation at least up to 1500 K, owing to double π/σ aromaticity.

Conflicts of interest

There are no conflicts to declare.

Acknowledgements

This work was supported by the National Natural Science Foundation of China (21873058, 21573138) and the Sanjin Scholar Distinguished Professors Program.

References

1 B. Albert and H. Hillebrecht, *Angew. Chem., Int. Ed.*, 2009, **48**, 8640.
2 A. J. Mannix, X. F. Zhou, B. Kiraly, J. D. Wood, D. Alducin, B. D. Myers, X. Liu, B. L. Fisher, U. Santiago, J. R. Guest, M. J. Yacaman, A. Ponce, A. R. Oganov, M. C. Hersam and N. P. Guisinger, *Science*, 2015, **350**, 1513.
3 B. Feng, J. Zhang, Q. Zhong, W. Li, S. Li, H. Li, P. Cheng, S. Meng, L. Chen and K. Wu, *Nat. Chem.*, 2016, **8**, 563.
4 H. J. Zhai, Y. F. Zhao, W. L. Li, Q. Chen, H. Bai, H. S. Hu, Z. A. Piazza, W. J. Tian, H. G. Lu, Y. B. Wu, Y. W. Mu, G. F. Wei, Z. P. Liu, J. Li, S. D. Li and L. S. Wang, *Nat. Chem.*, 2014, **6**, 727.
5 A. N. Alexandrova, A. I. Boldyrev, H. J. Zhai and L. S. Wang, *Coord. Chem. Rev.*, 2006, **250**, 2811.
6 A. P. Sergeeva, I. A. Popov, Z. A. Piazza, W. L. Li, C. Romanescu, L. S. Wang and A. I. Boldyrev, *Acc. Chem. Res.*, 2014, **47**, 1349.
7 E. Oger, N. R. M. Crawford, R. Kelting, P. Weis, M. M. Kappes and R. Ahlrichs, *Angew. Chem., Int. Ed.*, 2007, **46**, 8503.
8 J. O. C. Jiménez-Halla, R. Islas, T. Heine and G. Merino, *Angew. Chem., Int. Ed.*, 2010, **49**, 5668.
9 H. J. Zhai, A. N. Alexandrova, K. A. Birch, A. I. Boldyrev and L. S. Wang, *Angew. Chem., Int. Ed.*, 2003, **42**, 6004.
10 H. J. Zhai, B. Kiran, J. Li and L. S. Wang, *Nat. Mater.*, 2003, **2**, 827.
11 J. C. Guo, L. Y. Feng, Y. J. Wang, S. Jalife, A. Vásquez-Espinal, J. L. Cabellos, S. Pan, G. Merino and H. J. Zhai, *Angew. Chem., Int. Ed.*, 2017, **56**, 10174.
12 W. Huang, A. P. Sergeeva, H. J. Zhai, B. B. Averkiev, L. S. Wang and A. I. Boldyrev, *Nat. Chem.*, 2010, **2**, 202.
13 Y. J. Wang, X. Y. Zhao, Q. Chen, H. J. Zhai and S. D. Li, *Nanoscale*, 2015, **7**, 16054.
14 Q. Chen, W. L. Li, Y. F. Zhao, S. Y. Zhang, H. S. Hu, H. Bai, H. R. Li, W. J. Tian, H. G. Lu, H. J. Zhai, S. D. Li, J. Li and L. S. Wang, *ACS Nano*, 2015, **9**, 754.
15 Y. J. Wang, Y. F. Zhao, W. L. Li, T. Jian, Q. Chen, X. R. You, T. Ou, X. Y. Zhao, H. J. Zhai, S. D. Li, J. Li and L. S. Wang, *J. Chem. Phys.*, 2016, **144**, 064307.
16 V. Bezugly, J. Kunstmann, B. Grundkötter-Stock, T. Frauenheim, T. Niehaus and G. Cuniberti, *ACS Nano*, 2011, **5**, 4997.
17 A. van Orden and R. J. Saykally, *Chem. Rev.*, 1998, **98**, 2313.
18 S. Yang, K. J. Taylor, M. J. Craycraft, J. Conceicao, C. L. Pettiette, O. Cheshnovsky and R. E. Smalley, *Chem. Phys. Lett.*, 1988, **144**, 431.
19 Q. S. Li and Q. Jin, *J. Phys. Chem. A*, 2004, **108**, 855.
20 L. M. Molina, M. J. López, I. Cabria, J. A. Alonso and N. H. March, *Phys. Rev. B: Condens. Matter Mater. Phys.*, 2005, **72**, 113414.
21 Z. H. Cui, W. S. Yang, L. Zhao, Y. H. Ding and G. Frenking, *Angew. Chem., Int. Ed.*, 2016, **55**, 7841.
22 G. Martínez-Guajardo, A. P. Sergeeva, A. I. Boldyrev, T. Heine, J. M. Ugalde and G. Merino, *Chem. Commun.*, 2011, **47**, 6242.
23 J. Zhang, A. P. Sergeeva, M. Sparta and A. N. Alexandrova, *Angew. Chem., Int. Ed.*, 2012, **51**, 8512.
24 D. Moreno, S. Pan, L. L. Zeonjuk, R. Islas, E. Osorio, G. Martínez-Guajardo, P. K. Chattaraj, T. Heine and G. Merino, *Chem. Commun.*, 2014, **50**, 8140.
25 F. Cervantes-Navarro, G. Martínez-Guajardo, E. Osorio, D. Moreno, W. Tiznado, R. Islas, K. J. Donald and G. Merino, *Chem. Commun.*, 2014, **50**, 10680.
26 Y. J. Wang, X. R. You, Q. Chen, L. Y. Feng, K. Wang, T. Ou, X. Y. Zhao, H. J. Zhai and S. D. Li, *Phys. Chem. Chem. Phys.*, 2016, **18**, 15774.
27 S. Jalife, L. Liu, S. Pan, J. L. Cabellos, E. Osorio, C. Lu, T. Heine, K. J. Donald and G. Merino, *Nanoscale*, 2016, **8**, 17639.
28 Y. J. Wang, J. C. Guo and H. J. Zhai, *Nanoscale*, 2017, **9**, 9310.
29 M. R. Fagiani, X. Song, P. Petkov, S. Debnath, S. Gewinner, W. Schöllkopf, T. Heine, A. Fielicke and K. R. Asmis, *Angew. Chem., Int. Ed.*, 2017, **56**, 501.
30 Y. J. Wang, L. Y. Feng, J. C. Guo and H. J. Zhai, *Chem. – Asian J.*, 2017, **12**, 2899.
31 A. I. Boldyrev and L. S. Wang, *Phys. Chem. Chem. Phys.*, 2016, **18**, 11589.
32 J. K. Olson and A. I. Boldyrev, *Chem. Phys. Lett.*, 2012, **523**, 83.
33 X. Zhang, K. A. Lundell, J. K. Olson, K. H. Bowen and A. I. Boldyrev, *Chem. – Eur. J.*, 2018, DOI: 10.1002/chem.201800517.
34 K. A. Lundell, X. Zhang, A. I. Boldyrev and K. H. Bowen, *Angew. Chem., Int. Ed.*, 2017, **56**, 16593.
35 I. A. Popov, X. Zhang, B. W. Eichhorn, A. I. Boldyrev and K. H. Bowen, *Phys. Chem. Chem. Phys.*, 2015, **17**, 26079.
36 A. S. Ivanov, A. J. Morris, K. V. Bozhenko, C. J. Pickard and A. I. Boldyrev, *Angew. Chem., Int. Ed.*, 2012, **51**, 8330.
37 D. Pfister, K. Schäfer, C. Ott, B. Gerke, R. Pöttgen, O. Janka, M. Baumgartner, A. Efimova, A. Hohmann, P. Schmidt, S. Venkatachalam, L. v. Wüllen, U. Schürmann, L. Kienle, V. Duppel, E. Parzinger, B. Miller, J. Becker, A. Holleitner, R. Weihrich and T. Nilges, *Adv. Mater.*, 2016, **28**, 9783.
38 A. P. Sergeeva, B. B. Averkiev, H. J. Zhai, A. I. Boldyrev and L. S. Wang, *J. Chem. Phys.*, 2011, **134**, 224304.
39 M. Saunders, *J. Comput. Chem.*, 2004, **25**, 621.
40 P. P. Bera, K. W. Sattelmeyer, M. Saunders, H. F. Schaefer III and P. v. R. Schleyer, *J. Phys. Chem. A*, 2006, **110**, 4287.
41 S. Goedecker, *J. Chem. Phys.*, 2004, **120**, 9911.
42 S. Goedecker, W. Hellmann and T. Lenosky, *Phys. Rev. Lett.*, 2005, **95**, 055501.
43 C. Adamo and V. Barone, *J. Chem. Phys.*, 1999, **110**, 6158.
44 J. A. Pople, M. Head-Gordon and K. Raghavachari, *J. Chem. Phys.*, 1987, **87**, 5968.
45 G. E. Scuseria, C. L. Janssen and H. F. Schaefer III, *J. Chem. Phys.*, 1988, **89**, 7382.
46 G. E. Scuseria and H. F. Schaefer III, *J. Chem. Phys.*, 1989, **90**, 3700.

47 D. Y. Zubarev and A. I. Boldyrev, *Phys. Chem. Chem. Phys.*, 2008, **10**, 5207.
48 A. E. Reed, L. A. Curtiss and F. Weinhold, *Chem. Rev.*, 1988, **88**, 899.
49 E. D. Glendening, J. K. Badenhoop, A. E. Reed, J. E. Carpenter, J. A. Bohmann, C. M. Morales, C. R. Landis and F. Weinhold, *NBO 6.0*, Theoretical Chemistry Institute, University of Wisconsin, Madison, 2013.
50 T. Lu and F. W. Chen, *Acta Chim. Sin.*, 2011, **69**, 2393.
51 Z. Chen, C. S. Wannere, C. Corminboeuf, R. Puchta and P. v. R. Schleyer, *Chem. Rev.*, 2005, **105**, 3842.
52 J. VandeVondele, M. Krack, F. Mohamed, M. Parrinello, T. Chassaing and J. Hutter, *Comput. Phys. Commun.*, 2005, **167**, 103.
53 U. Varetto, *Molekel 5.4.0.8*, Swiss National Supercomputing Center, Manno, Switzerland, 2009.
54 M. J. Frisch, *et al.*, *Gaussian 09, revision D.01*, Gaussian Inc., Wallingford, Connecticut, 2009.
55 P. Pyykkö, *J. Phys. Chem. A*, 2015, **119**, 2326.
56 L. B. Knight, K. Kerr, P. K. Miller and C. A. Arrington, *J. Phys. Chem.*, 1995, **99**, 16842.
57 G. Treboux and J. C. Barthelat, *J. Am. Chem. Soc.*, 1993, **115**, 4870.
58 J. D. Dill, P. v. R. Schleyer and J. A. Pople, *J. Am. Chem. Soc.*, 1975, **97**, 3402.
59 A. Kalemos, *J. Chem. Phys.*, 2016, **145**, 214302.
60 Structure **TS1** is related to GM **1**, following in-planar rotation of the outer B_{10} ring against the Be_6 prism by half a B–B link. Note that the B–B and Be–Be distances in **TS1** closely resemble those in GM **1**, hinting at structural fluxionality for cluster **1**. Likewise, **TS2** corresponds to structural transformation from GM **1** to LM **3**, suggesting another possible dynamic mode.
61 In this alternative AdNDP scheme, the contribution from the Be_6 prism is omitted, leading to minor decreases in occupation numbers (ONs) by less than 15%. Thus, $10\pi/10\sigma$ subsystems in cluster **1** are indeed dominated by the outer B_{10} ring.
62 S. Dapprich and G. Frenking, *J. Phys. Chem.*, 1995, **99**, 9352.
63 To accommodate a reviewer, we ran complementary CDA calculations[62] for the charge transfer complex. Specifically, we divide the $Be_6B_{10}^{2-}$ cluster into Be_6^{8+} and B_{10}^{10-} segments, and the CDA results point to a final formula of $[Be_3]^{4.63+}[B_{10}]^{6.63-}$, which is qualitatively consistent with a charge transfer cluster, although the quantitative number of electrons transferred is less than those in the formal (8 $|e|$) and NBO (6.56 $|e|$) data. We consider the formal picture of $[Be_3]^{4+}[B_{10}]^{10-}[Be_3]^{4+}$ from CMO analyses to be fundamental, which is confirmed by AdNDP and NBO analyses. In this context, the CDA data are relatively unimportant (and indeed less reliable).
64 S. Martín-Santamaría and H. S. Rzepa, *Chem. Commun.*, 2000, 1503.
65 This argument is valid for two reasons. Firstly, the expansion of B–B distances in GM $Be_6B_{10}^{2-}$ (**1**) (Fig. 2(b)) relative to $Be_6B_{11}^{-}$ (C_{2v}, $^1A_1$) (Fig. S1(b), ESI†)[11] is not due to the dianion nature of **1**, because the neutral $Be_6B_{10}Na_2$ salt complex (Fig. S1(a), ESI†) follows the same trend. Second, species $Be_6B_{11}^{-}$ (C_{2v}, $^1A_1$), GM $Be_6B_{10}^{2-}$ (**1**), and LM $Be_6B_{10}^{2-}$ (**3**) (Fig. 4(a)) form a whole series, along which the B–B links expand systematically and the Be–Be links in the Be_3 rings shrink. Using the average values, the B–B/Be–Be bonds are 1.53/2.21, 1.57/2.11, and 1.58/2.09 Å, respectively, suggesting that geometric constraints increase monotonously along the series and size mismatch between the B_{10} and Be_3 rings does exist in GM $Be_6B_{10}^{2-}$ (**1**). Such mismatch is relevant to the energy barrier for the twisting mode.